ACS APPLIED MATERIALS & INTERFACES

Research Article

www.acsami.org

Copper-Based Conductive Composites with Tailored Thermal Expansion

Enrico Della Gaspera,[†,∥] Ryan Tucker,[†] Kurt Star,[†,‡] Esther H. Lan,[†] Yongho Sungtaek Ju,[§] and Bruce Dunn*[,†]

[†]Department of Materials Science and Engineering, University of California Los Angeles, 420 Westwood Plaza, Los Angeles, California 90095-1595, United States

[‡]Materials and Device Technology, Jet Propulsion Laboratory, Pasadena, California 91109, United States

[§]Department of Mechanical and Aerospace Engineering, University of California Los Angeles, 420 Westwood Plaza, Los Angeles, California 90095-1595, United States

Supporting Information

ABSTRACT: We have devised a moderate temperature hot-pressing route for preparing metal−matrix composites which possess tunable thermal expansion coefficients in combination with high electrical and thermal conductivities. The composites are based on incorporating ZrW_2O_8, a material with a negative coefficient of thermal expansion (CTE), within a continuous copper matrix. The ZrW_2O_8 enables us to tune the CTE in a predictable manner, while the copper phase is responsible for the electrical and thermal conductivity properties. An important consideration in the processing of these materials is to avoid the decomposition of the ZrW_2O_8 phase. This is accomplished by using relatively mild hot-pressing conditions of 500 °C for 1 h at 40 MPa. To ensure that these conditions enable sintering of the copper, we developed a synthesis route for the preparation of Cu nanoparticles (NPs) based on the reduction of a common copper salt in aqueous solution in the presence of a size control agent. Upon hot pressing these nanoparticles at 500 °C, we are able to achieve 92−93% of the theoretical density of copper. The resulting materials exhibit a CTE which can be tuned between the value of pure copper (16.5 ppm/°C) and less than 1 ppm/°C. Thus, by adjusting the relative amount of the two components, the properties of the composite can be designed so that a material with high electrical conductivity and a CTE that matches the relatively low CTE values of semiconductor or thermoelectric materials can be achieved. This unique combination of electrical and thermal properties enables these Cu-based metal−matrix composites to be used as electrical contacts to a variety of semiconductor and thermoelectric devices which offer stable operation under thermal cycling conditions.

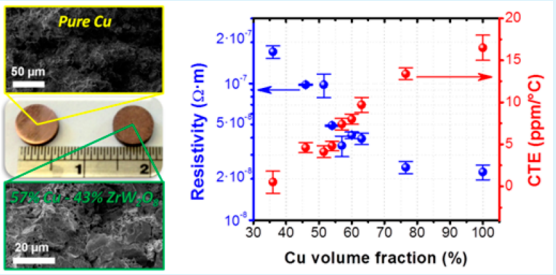

KEYWORDS: *nanoparticles, colloidal synthesis, negative thermal expansion, zirconium tungstate, sintering, electrical properties*

INTRODUCTION

Thermomechanical reliability of electrical contacts is one of the major issues facing the development of high performance semiconductors and thermoelectric-based devices.[1,2] The interfaces formed between the active materials and the structures with which they are integrated are a source of mechanical stresses during thermal cycling as a consequence of the mismatch in thermal expansion occurring in such junctions. These stresses are often responsible for poor performance of the device or even its failure.[3] Traditional thermoelectric materials such as metal silicides (Mg_2Si or Fe_2Si for example) and semiconductors like gallium arsenide (GaAs) or indium phosphide (InP) have a coefficient of thermal expansion (CTE) substantially lower than the metals used as electrical contacts. For example, the CTE of Mg_2Si is around 7.5 ppm/°C,[4,5] while the CTE for Fe_2Si varies between 6.8 and 10 ppm/°C according to the crystalline phase and the preparation technique.[6,7] Many semiconductors have an even lower CTE. For example, the room-temperature values for GaAs and InP are ∼5.8 ppm/°C and 4.6 ppm/°C, respectively.[8−11] By comparison, highly conductive metals such as Ag and Cu have a much larger CTE, 18.9 ppm/°C for Ag and 16.5 ppm/°C for Cu.[12]

Establishing a proper contact interface, where a highly conductive material with an appropriate CTE is joined to the active semiconductor or thermoelectric, is of paramount importance to maximize the performance and operational life of the target device. Unfortunately, a very conductive and relatively inexpensive material with low thermal expansion does not exist. Composites, on the other hand, offer the opportunity to design and fabricate materials with tailored properties by combining two or more different components where each

Received: August 4, 2013
Accepted: October 15, 2013
Published: October 31, 2013

constituent provides a certain property to the final composite.[13,14]

Our approach to creating a material with high electrical conductivity and low CTE involves the development of metal-based composites in which a negative thermal expansion oxide is embedded within a metal matrix. The continuous metal matrix is responsible for achieving the desired electrical and thermal conductivity properties, while the presence of the oxide allows the tailoring of the CTE to match the value of the active semiconductor or thermoelectric material. By adjusting the relative amount of the two components, the properties of the composite can be designed so that a material with high electrical conductivity and desired CTE can be realized.

Metal matrix composites have been studied extensively. Combining ceramic reinforcements and a metallic matrix enables one to tailor and improve the properties of the composite in terms of hardness, fracture toughness, thermal expansion, thermal and electrical conductivity, etc. The processing, properties, and modeling of metal−matrix composites and their technological applications have been reviewed.[14,15] A number of studies on thermal expansion of metal−matrix composites have been carried out in which a range of parameters including the amount, size, and shape of different fillers, processing approaches, and thermal cycling behavior have been investigated and led to models aimed at predicting and estimating composite properties.[16−18]

In the present study, we selected zirconium tungstate (ZrW_2O_8) as the oxide filler due to its isotropic negative thermal expansion over a wide temperature range.[19,20] This material exists in different crystalline phases: in particular the cubic α-phase has a distinctive structure that can be described as an alternation of WO_4 tetrahedra and ZrO_6 octahedra bridged by oxygen atoms shared at the corners. The structure is slightly asymmetric because each ZrO_6 octahedron shares all six of its oxygen corner atoms with six WO_4 tetrahedra, while each WO_4 tetrahedron shares only three of its four oxygen atoms with adjacent ZrO_6 octahedra. The negative thermal expansion of this compound is due to transverse vibrations of Zr−O−W bonds that cause a shrinkage in the lattice with increasing temperature. Reported CTE values for this material vary between −8.7 ppm/°C and −9.1 ppm/°C up to about 160 °C.[20,21] If heated above this temperature, it undergoes a phase transition to a slightly disordered state (the cubic β-phase) that causes the CTE to increase, although the material still has a negative CTE (−4.9 ppm/°C).[19,22] This phase transition is completely reversible, and the α-phase is restored upon cooling the material below the transition temperature. Zirconium tungstate begins decomposing into WO_3 and ZrO_2 after prolonged heating at 600 °C,[23] thus limiting the processing temperature for composite preparation. In addition, amorphization of the cubic α-phase is found to occur when high pressures are applied. At intermediate pressures the α-phase can transform into the orthorhombic γ-phase.[24−26] This phase also exhibits a negative CTE, although not as prominent as the cubic phases (around −1 ppm/°C).[27] For these reasons, a processing procedure that uses mild conditions with respect to both temperature and pressure is necessary to avoid decomposition or transformation of the zirconium tungstate and achieve reliable and reproducible expansion behavior in the hot-pressed composites.

The use of ZrW_2O_8 in metal−matrix composites has been reported previously. Although a tunable CTE was observed as a function of ceramic loading, the results were not fully reproducible as a consequence of the decomposition and/or irreversible transformation of zirconium tungstate during composite fabrication.[28] Prior research on the Cu−ZrW_2O_8 system is especially relevant to the study reported here. Because of these irreversible reactions, the thermal expansion results shown in the earlier work were fairly scattered, with the measured CTE not following any specific trend with composite composition or being substantially different from the predicted value.[29,30] These studies also identified the decomposition and/or phase transformation products and the operative window to avoid such reactions.

Other studies on this topic focus on simulating and modeling composite behavior and analyzing the effect of thermal cycling (temperatures, heating and cooling rate) on the thermal and mechanical properties of the composites.[31]

We recently reported a silver−zirconium tungstate composite using Ag nanoparticles (NPs) as the silver source.[32] The use of nanosized metallic powders enables lower processing temperatures for composite preparation because the melting and sintering temperatures for nearly all metals decrease with decreasing particle size.[33−36] We were able to obtain a tunable CTE with good reproducibility, but because of the high cost of silver, Ag−ZrW_2O_8 composites represent a proof of concept experiment which is unlikely to provide practical solutions to the electrical contact issues mentioned above.

In the present work, copper was selected as the metal for the matrix because of its high conductivity and its greater practicality compared to silver. The electrical conductivity of Cu, 5.96×10^7 S/m, is greater than that of other metals often used in metal−matrix composites, such as aluminum and nickel (3.7×10^7 S/m and 1.44×10^7 S/m, respectively).[37] Moreover, copper is attractive because of its high thermal conductivity. The fact that the melting temperature of copper (1084 °C) is not very high means that it should be compatible with hot pressing at temperatures below the decomposition temperature of ZrW_2O_8. As observed previously for Ag, to achieve a completely sintered material at temperatures and pressures compatible with the thermal stability of zirconium tungstate, the copper particles need to be in the nanometer size range. Accordingly, we developed a straightforward route to synthesize small (∼5 nm diameter) Cu NPs using colloidal techniques. The particles are then purified, dried, and used for composite preparation together with ZrW_2O_8 powders synthesized using a previously published procedure.[38] High quality composite pellets with tunable CTE and good electrical and thermal properties are synthesized using hot pressing under relatively mild conditions (500 °C, 40 MPa, 1 h) which avoid the decomposition of ZrW_2O_8.

EXPERIMENTAL SECTION

Materials and Methods. All chemicals are of reagent grade and used without any further purification. Cu NPs are synthesized by adapting a synthetic route reported for ∼3 nm Au NPs.[39] Copper sulfate pentahydrate ($CuSO_4{\cdot}5H_2O$) and poly(*N*-vinylpyrrolidone) of 10 000 g/mol average molecular weight (PVP) are dissolved in water to give a Cu concentration of 25 mM and a ratio of gPVP/mol Cu = 900. Cu^{2+} ions are reduced to metallic copper using a freshly prepared aqueous solution of sodium borohydride ($NaBH_4$). The $NaBH_4$ concentration in the reducing solution is kept to 0.8 M, and the $NaBH_4$/Cu molar ratio is fixed at 8. In a typical synthesis, 1.25 g of $CuSO_4{\cdot}5H_2O$ and 4.5 g of PVP are dissolved in 200 mL of deionized water. Separately, 1.5 g of $NaBH_4$ is dissolved in 50 mL of deionized water. The sodium borohydride solution is poured in less than 1 s into

the copper solution under strong stirring, causing a rapid change in color from pale blue to deep brown, indicating copper NP formation.

CAUTION: sodium borohydride is highly reactive, and the reaction with metal salts causes hydrogen gas release[40] creating a foaming solution due to the presence of PVP. The foam disappears in about 20−30 s. The use of large containers (beakers or crystallizing dishes) rather than narrow vials or Erlenmeyer flasks is advised to let the foam evolve and settle quickly and to avoid solution leaking or overflowing in the initial stages of the reaction. After the introduction of sodium borohydride the containers should never be closed tightly for at least a few hours to allow residual gas evolution. Proper protective equipment must be worn at all times, and the procedure has to be performed in a ventilated fume hood.

A few minutes after the sodium borohydride addition, the colloidal solutions are transferred into glass bottles and allowed to stand without stirring. Aggregation of the NPs occurs, and a precipitate is observed within 24−48 h. The clear supernatant is removed, and the particles are redispersed in water and centrifuged at 4000 rpm for 5 min. This washing procedure is repeated at least 3 times to remove reaction byproducts, unreacted precursors, and excess PVP. Acetone is used for the last washing, and the particles are eventually dried at room temperature under vacuum for 5 h, ground with a mortar and pestle, and kept in a sealed vial for further use.

ZrW_2O_8 powder in the cubic α-phase is synthesized as reported elsewhere.[38] Briefly, zirconium oxychloride octahydrate ($ZrOCl_2 \cdot 8H_2O$) and ammonium tungstate hydrate ($(NH_4)_6H_2W_{12}O_{40} \cdot xH_2O$) are dissolved in water in the presence of citric acid using a molar ratio Zr:W:acid = 1:2:6. Ammonium hydroxide (30%) is used to adjust the solution to about pH 7. The solution is transferred into an oven at 60 °C for approximately 20 h until a viscous gel is formed. The gel is subsequently annealed at 800 °C for 12 h to remove organic components. The resulting powder is then sintered at 1180 °C for 2 h followed by immediate quenching in liquid nitrogen to preserve the desired oxide phase. The synthesized ZrW_2O_8 is then finely ground and stored for further use.

Since copper NPs are fairly reactive, their surface slowly oxidizes at room temperature to Cu_2O (see Results and Discussion section for details). Thus, before hot pressing takes place, the as-synthesized Cu@Cu_2O NPs are completely reduced to metallic Cu by heating to 200−250 °C in a tube furnace for 2 h under forming gas (5% H_2−95% Ar). The ZrW_2O_8 and reduced Cu powders are then mixed and ground together in an agate mortar according to the desired ratio. Composites containing up to 50 wt % of oxide filler were prepared. The range of compositions is shown in Table S1 in the Supporting Information. The mixed powders were loaded into a graphite die and hot pressed at 40 MPa in a home-built hot press at 500 °C for 1 h under a forming gas atmosphere. Details of the hot press apparatus are reported elsewhere.[41]

Characterization Techniques. Transmission electron microscopy (TEM) measurements of the NPs deposited on a carbon-coated copper grid were taken with an FEI Technai T12 TEM. The NP size distribution was determined using Fiji-Image J 1.44b image analyzer software[42] counting at least 100 particles. Dry powder samples and composite pellets were characterized by X-ray diffraction (XRD) by using a Rigaku Miniflex II diffractometer equipped with a Cu Kα radiation source. Optical absorption spectra of solutions were measured using a Varian-Cary 100 Bio UV−vis spectrophotometer. Thermogravimetric analysis (TGA) was performed in either air or argon atmosphere using a TA SDT Q600 analyzer at a heating rate of 5 °C/min. The density of the pressed pellets was determined by the Archimedes method using a Mettler Toledo Excellence XP/XS precision balance density kit, and a Fei Nova NanoSEM 230 scanning electron microscope (SEM) was used to characterize composite microstructure. A Netzsch DIL 402PC dilatometer was used to measure the CTE of the prepared composites under an Ar atmosphere. Electrical conductivity was measured by the four-point van der Pauw method using a 100 mA current in a custom apparatus described elsewhere.[43] Thermal conductivity was measured with the laser flash and hot wire technique using a Netzsch LFA 447 Nanoflash instrument.

RESULTS AND DISCUSSION

1. Characterization of Cu Nanoparticles. We adapted a synthetic route used to prepare small (1−3 nm in diameter) Au NPs.[39] The method involves the rapid reduction of the metal salt in an appropriate solvent in the presence of a size-controlling agent, PVP. This polymer is widely known to bind to the surface of metal NPs with its N−C−O groups to thus provide efficient steric stabilization to even small and highly reactive colloids.[44,45] We carried out the synthesis in water to use a nontoxic solvent.

We used different PVP amounts and copper concentrations to obtain small and homogeneous particles at the highest concentration possible. The different experimental conditions used to optimize the synthesis are reported in Table S2 in the Supporting Information. Without using PVP, immediate aggregation occurs right after injecting the sodium borohydride solution, confirming the role of the polymer as a stabilizer for the colloidal solution. Similar effects of PVP presence on the stabilization of metal colloids have been observed previously.[46] Moreover, as already reported for different metallic NPs such as Ni,[47] Cu,[48] and Au,[39,45] the larger the ratio between PVP and the metal, the smaller the final NP size (Figure S1, Supporting Information). As a result, our Cu NP synthesis is more than 10 times more concentrated than similar low-temperature syntheses developed for Au[39,45] or Ag,[49,50] suggesting its feasibility for large-scale production.

The as-synthesized Cu NPs are about 5 nm in size, and over time their surface slowly oxidizes to cuprous oxide (Cu_2O) due to their large surface energy. This behavior has been widely observed for the colloidal synthesis of Cu NPs under an inert atmosphere:[51,52] as soon as the colloids are exposed to air or to an oxygen-containing environment, oxidation starts to occur. For this reason we decided to perform a direct synthesis in water, at room temperature and ambient atmosphere, and subsequently reduce the oxidized surface of the NPs at a later time but prior to hot pressing.

A TEM image of the Cu NPs drop cast onto a TEM grid 1 h after the synthesis is shown in Figure 1a. The image, taken

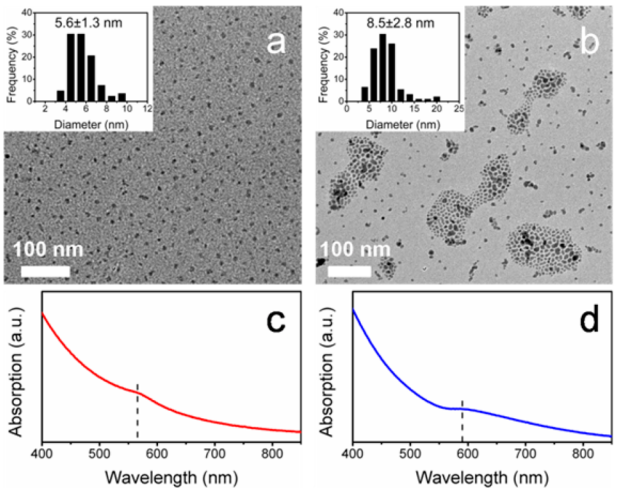

Figure 1. TEM images of the as-synthesized NPs (a) and the same NP batch aged at room temperature for about one month (b); the insets show the corresponding size distribution evaluated from TEM. Optical absorption spectra of the as-synthesized particles in water (c) and the aged particles in chloroform (d). The dashed vertical lines highlight the wavelengths corresponding to the SPR peak.

within one day after the grid preparation, shows the particles to be small and slightly polydisperse. The average size evaluated from TEM images is 5.6 ± 1.3 nm, as can be seen in the inset.

Figure 1b shows a TEM micrograph of Cu@Cu_2O NPs stabilized with oleic acid and kept in a chloroform solution for about one month (see Figure S2 in the Supporting Information for details). The particles are well dispersed on the grid, and due to the controlled evaporation of the solvent, they started to self-assemble in some two-dimensional structures. The size of the NPs in Figure 1b is slightly larger compared to the as-synthesized colloids (Figure 1a), possibly due to some oxidation-driven growth and Ostwald ripening processes occurring over time.

Figure 1 also compares the optical absorption spectra of the NPs synthesized in water (Figure 1c) with those aged for one month in chloroform after being protected with oleic acid (Figure 1d). The spectrum in Figure 1c for the as-prepared NPs shows a weak surface plasmon resonance (SPR) peak centered at about 560 nm and a diffuse absorption typically observed in very small (few nanometers) metallic particles.[53] As the oxidation proceeds, the SPR peak red shifts as a consequence of the greater refractive index of the oxide shell with respect to the solvent[54] and becomes asymmetric at longer wavelengths due to the superposition of the exciton peak of cuprous oxide centered at about 700 nm,[52] as can be seen in Figure 1d.

Following the washing protocols described previously, the particles are dried and stored as a powder for further use. XRD analyses on such dried powders have been carried out to evaluate the different crystalline phases in the synthesized nanoparticles. The results are presented in Figure 2a. In the case of as-synthesized NPs, measurements are taken within 3−4 days after the synthesis due to the time necessary to wash, purify, and dry the NPs. These materials are mainly composed of metallic Cu with a very small Cu_2O shell. In fact all the diffraction peaks can be assigned to cubic Cu (JCPDS no. 85-1326) and to cubic Cu_2O (JCPDS no. 78-2076). The amount of cuprous oxide is fairly low, as confirmed from the broad, weak peak at about 36.5° in scan A of Figure 2a. This behavior is consistent with there being a mild oxidation at the surface of Cu NPs during the first few days after synthesis. The Cu crystallite size evaluated using the Scherrer relationship for the as-synthesized NPs is 6.1 ± 0.3 nm, while the Cu_2O crystallite size is 3.2 ± 0.4 nm, in reasonable agreement with TEM data. Prolonged exposure to oxidizing atmosphere (air) leads to further oxidation of Cu to Cu_2O, as can be seen from pattern B, where the oxide peaks become predominant with respect to the metallic ones. We observed a non-negligible increase in crystallite size up to 9.5 ± 1.0 nm for Cu and 12.4 ± 1.2 nm for Cu_2O, suggesting a progressive oxidation-driven growth over time even at room temperature. There is no evidence of CuO formation at least after keeping the dry powders at room temperature for up to two months.

Prior to hot pressing, the Cu@Cu_2O powders are reduced at 250 °C in forming gas. This procedure avoids gas evolution and the formation of oxide residues as a consequence of the in situ reduction of Cu_2O to Cu during the hot pressing. After the reducing treatment, the resulting powders are metallic Cu without any indication of oxide or other impurities, as shown in scan C.

Even though the crystallite size increased to 21.1 ± 4.8 nm, this increase is not dramatic and does not affect the sintering properties, as will be presented in Section 3.

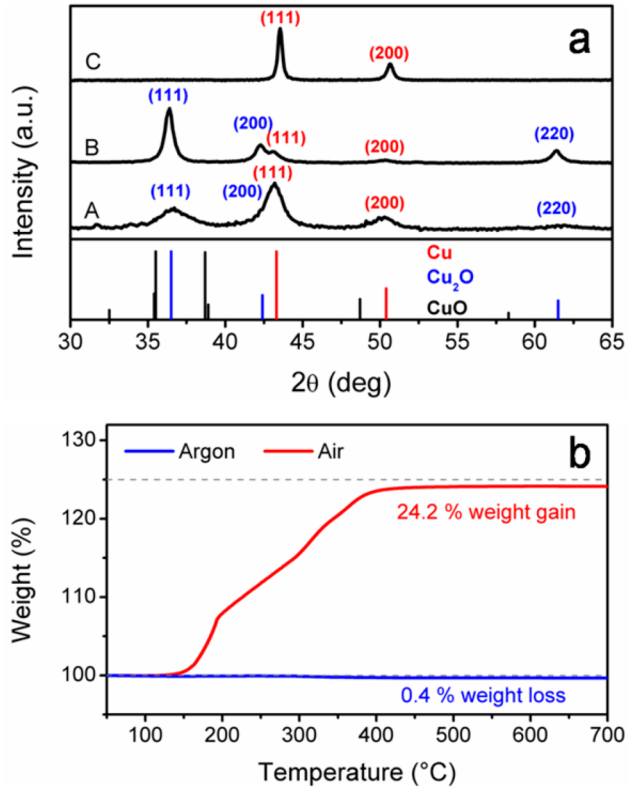

Figure 2. (a) XRD patterns of the prepared samples: (A) as-synthesized NPs; (B) Cu@Cu_2O powders aged at room temperature for several weeks; (C) Cu NPs after the annealing in forming gas atmosphere at 250 °C. Diffraction peak positions for Cu (red), Cu_2O (blue), and CuO (black) are also reported. (b) TGA of the Cu powders reduced at 250 °C in forming gas, performed in argon (blue line) and in air (red line); the gray dashed lines highlight 100% and 125% weight, corresponding to no weight loss and to full oxidation of Cu to CuO, respectively.

TGA was also performed to evaluate the amount of residual organic material on the surface of the prepared powders after the washing procedure and the forming gas annealing step. The results shown in Figure 2b indicate that annealing in an inert atmosphere causes almost no weight loss or gain, suggesting that the starting powders are metallic Cu, without any organic contaminants (blue line in Figure 2b). This is desirable for our application, where a dense, sintered, and fully inorganic pellet has to be obtained. When performing the TGA under oxidizing conditions (air, red line in Figure 2b), there is a substantial weight gain (+24.2%) that corresponds almost exactly to full oxidation from metallic Cu to CuO. Here, too, there is no evidence of organic compounds as their presence would cause a weight loss.

2. ZrW_2O_8 Characterization. We followed a published synthetic procedure to prepare micrometer-sized ZrW_2O_8 particles in the cubic α-phase.[38] Initially we started preparing nanosized zirconium tungstate using solvothermal routes to synthesize a hydrated form with low-temperature annealing to convert it into cubic ZrW_2O_8[55] (for details, see Figure S3 in the Supporting Information). However, it has been reported recently that nanocrystalline powders of zirconium tungstate suffer from "autohydration" reactions, a problem that is not encountered in micrometer-sized particles.[56] Another recent study shows that smaller ZrW_2O_8 nanoparticles have a greater propensity for hydration compared to larger particles.[57] For this

reason, we decided to move to another synthetic route that produces larger, but more stable, particles. The synthesized materials were analyzed by XRD to determine the crystalline phase and check for the presence of undesired products like WO_3 or ZrO_2. Pure, single-phase cubic zirconium tungstate (JCPDS no. 50-1868) in the α-phase is obtained after liquid nitrogen quenching of powders sintered at high temperature (plot A in Figure 3). Because zirconium tungstate starts

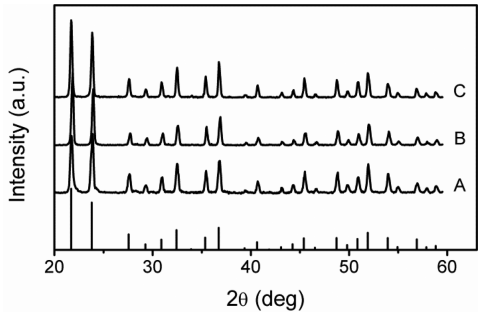

Figure 3. XRD patterns of zirconium tungstate powders: (A) as synthesized; (B) powders annealed at 575 °C for 4 h in air; (C) powders annealed at 500 °C for 3 h in forming gas. Diffraction peak positions for cubic α-ZrW_2O_8 are indicated at the bottom.

decomposing into tungsten and zirconium oxides above 600 °C, we investigated the stability of ZrW_2O_8 powders to prolonged annealing in air at temperatures as high as 575 °C. The XRD measurements show that there is no difference between these materials and the as-synthesized powders (scan B in Figure 3). In addition, the same powders were annealed in forming gas at 500 °C for up to 3 h to mimic the atmosphere conditions during hot pressing. Again, no difference in the XRD patterns can be detected (scan C in Figure 3).

3. Composite Pellet Characterization. *3.1. Microstructure Analysis.* Sintered pellets of pure Cu and a series of Cu–ZrW_2O_8 compositions with up to 50 wt % oxide filler were prepared by mixing a proper amount of the two powders and hot pressing them under reducing atmosphere (for details on pellet composition, refer to Table S1 in the Supporting Information). The average density of the prepared composite materials is about 85–90% compared to the expected theoretical density calculated as a linear combination of the densities of the pure materials, Cu and ZrW_2O_8, and averaged according to the respective volume fraction. Pure Cu pellets average 92–93% of theoretical density, while composite samples range from 75 to 94% of theoretical density depending upon composition (Figure 4 and Table S3 in the Supporting Information). The higher volume fractions of ZrW_2O_8 exhibit lower density. This behavior is not surprising considering that copper particles are responsible for the composite matrix and increasing the amount of oxide filler will make it more difficult to obtain a dense matrix surrounding the zirconium tungstate inclusions.

SEM cross sections of fracture surfaces were used to characterize the microstructure. Pellets were fractured after prolonged (~15 min) cooling in liquid nitrogen, and representative results are shown in Figure 5. By using fracture surfaces, we avoid any polishing which can be problematic in analyzing composite microstructures. Because Cu is very ductile at room temperature, polishing is likely to deform the metallic component in the composite surface and show apparent densification. Pure Cu pellets (Figure 5 a and b) show a

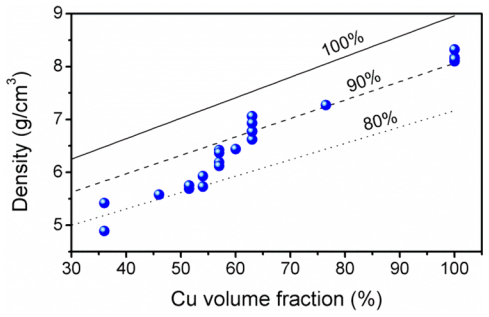

Figure 4. Density values as a function of the nominal Cu volume fraction for the prepared samples. The trends expected for 80%, 90%, and 100% of the theoretical density are based on using a linear combination of the theoretical densities for Cu and ZrW_2O_8.

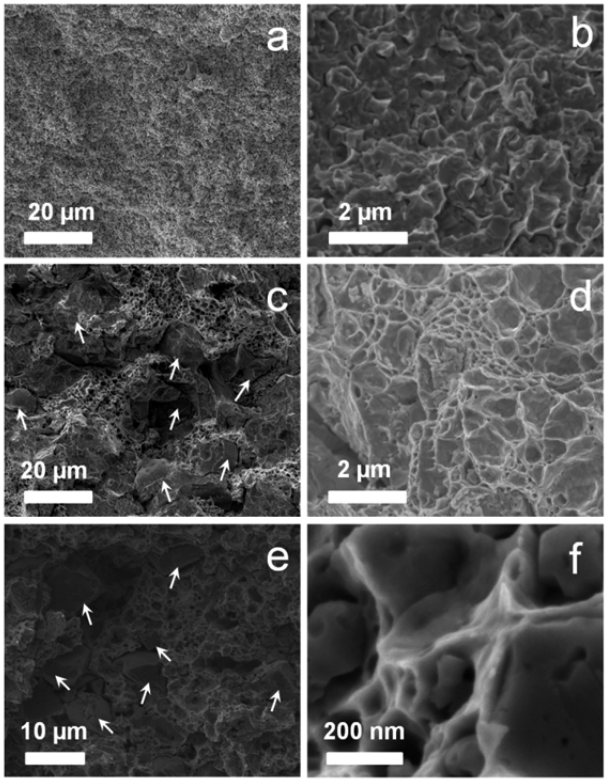

Figure 5. Cross-sectional SEM micrograph of a pure Cu pellet at different magnifications (a,b) and of a composite pellet containing 43 vol % of ZrW_2O_8 at different magnifications (c,d,e,f). The arrows highlight the zirconium tungstate particles.

homogeneous fracture surface over several tens of micrometers, without any change in morphology. The apparent roughness is possibly due to a transgranular fracture. SEM images of the composite pellets show that the zirconium tungstate microparticles are homogeneously dispersed within the copper matrix (Figure 5c and e). High magnification of the copper matrix of the composite pellet (Figure 5f) indicates that the metal matrix is fully sintered. These microstructures confirm the high quality of the prepared samples and lead to good agreement between calculated and measured CTE data.

XRD scans performed on sintered pellets show pure Cu and ZrW_2O_8 peaks, without the presence of any copper oxide, zirconium oxide, or tungsten oxide phases (Figure S4 in the Supporting Information). A certain amount of the ortho-

rhombic γ-phase of zirconium tungstate is also detected: this has been observed previously, and its existence is not surprising considering the large compressive stresses arising in the composites during cooling from the mismatch in thermal expansion (the Cu matrix contracts while the ZrW_2O_8 inclusions expand).[58,59] The orthorhombic phase possesses a negative CTE,[27] and is stable after prolonged thermal cycling as discussed in the next section. Thus, the presence of the orthorhombic phase has a minor effect on the thermal expansion behavior of the composites.

3.2. Thermal Expansion. Dilatometry measurements were used to determine the dimensional changes for samples cycled between room temperature and 300 °C. Every sample underwent at least three heating/cooling cycles, and the CTE for every sample was averaged for at least five measurements. Each data point in Figure 6a corresponds to the average value

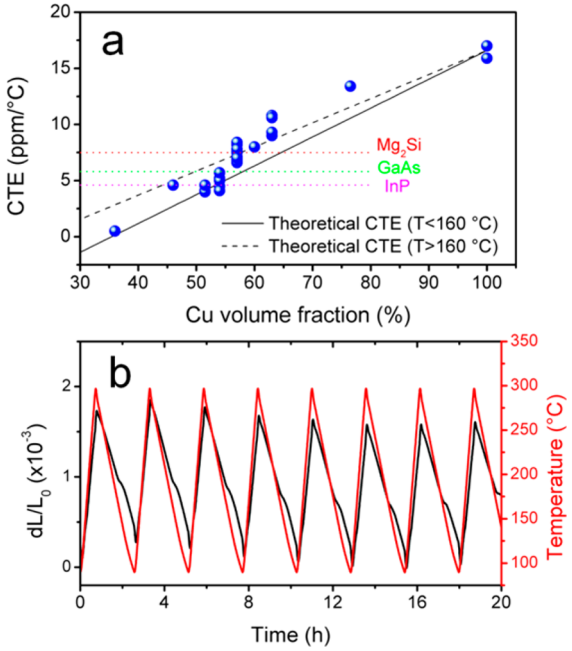

Figure 6. (a) Average CTE in the 80−300 °C range as a function of the Cu volume fraction for the prepared samples. The calculated CTE values are based on using a linear combination of the CTE for Cu and the two different CTE values for ZrW_2O_8 below and above 160 °C. These are highlighted with straight and dashed lines, respectively. The CTE values for Mg_2Si, GaAs, and InP are also shown. (b) Variation in length of a sample containing 43 vol % ZrW_2O_8 during repeated heating/cooling cycles: the heating rate is 5 °C/min, while the cooling rate is 2 °C/min. The average CTE is 7.1 ppm/°C.

for a single sample (the CTE values for each sample using one standard deviation as error bars are reported in Table S4 in the Supporting Information). There is reasonable agreement between the measured thermal expansion and the expected CTE based on the simple linear combination of each component. As discussed in the introduction, ZrW_2O_8 is known to have an isotropic negative thermal expansion over a wide temperature range (0.3−1050 K) with a phase transition at about 430 K (~160 °C). This phase transition leads to a decrease in the absolute value of the CTE, from about −9 ppm/°C for temperatures below 160 °C to about −4.9 ppm/°C for temperatures above 160 °C.[20] For this reason, two theoretical linear combinations are reported in Figure 6a. It seems that for low zirconium tungstate loading the contribution of the copper matrix is predominant, as the measured CTE values are larger than the expected ones; nonetheless, when the ZrW_2O_8 amount exceeds roughly 40 vol %, the trend in the CTE falls within the expected range. As mentioned above, a secondary orthorhombic phase which possesses a less negative CTE of about −1 ppm/°C is present in the composite. The presence of this phase will lead to a slight increase in the expected CTE for the composites, but this effect can be neglected for several reasons. First, the majority of the zirconium tungstate remains in the cubic phase even at room temperature. Moreover, most of the prepared samples contain at least 50% Cu, so the presence of the secondary γ-phase has a minor effect on the CTE of the composites. Finally, it is interesting to note that research on Al-ZrW_2O_8 composites showed that the orthorhombic phase converts back to cubic when the pellets are slightly heated.[60] A number of samples were remeasured after the initial CTE measurements, having been stored for at least 2 weeks at room temperature in air between each measurement. No substantial differences were observed, as the average CTE value is within the error bars (see Table S4 in the Supporting Information).

XRD measurements on the composite pellets after thermal cycling between room temperature and 300 °C did not show any evidence of decomposition of zirconium tungstate or oxidation of the copper matrix (see Figure S5 in the Supporting Information). This result indicates that the different crystalline phases which coexist within the composites are stable over the temperature window that we investigated. Only the pure Cu sample shows a very small additional diffraction peak that can be assigned to Cu_2O. This phase could possibly arise from the presence of oxygen during CTE measurements. The amount of the orthorhombic ZrW_2O_8 phase that formed after thermal cycling is comparable to that of the as-prepared material. This behavior suggests that once the partial phase change induced by pressure occurs during composite fabrication, the composite pellets are stable and can withstand temperature variations without being subjected to further transformations.

The dilatometry results show that by selecting the proper ratio of the two components the CTE can be tuned between about 16.5 ppm/°C (pure copper) and less than 1 ppm/°C (composites with 65 vol % of ZrW_2O_8). Samples containing 43 vol % of ZrW_2O_8 match the CTE of Mg_2Si, one of the most widely studied thermoelectric materials (~7.5 ppm/°C), while composites containing 46−49 vol % of ZrW_2O_8 match the CTE of the well-known III−V semiconductors, GaAs and InP.

The difference in CTE associated with the phase transition of ZrW_2O_8 affects the thermal expansion behavior of the composites when crossing the transition temperature of 160 °C. This difference becomes measurable only by increasing the zirconium tungstate loading and is barely detectable for samples containing more than 60 vol % of Cu. Nonetheless, this behavior actually represents an advantage because we believe that having such a small variation in CTE when crossing the transition temperature, instead of an abrupt and large change, will improve composite reliability over repeated heating−cooling cycles. Figure 6b shows a series of thermal cycles between 90 and 300 °C for a sample containing 43 vol % ZrW_2O_8. Excellent reproducibility and stability are observed, suggesting that the synthesized composites might be suitable as electrical contacts for semiconductors or thermoelectric materials. The measured CTE for this particular sample averaged for all cycles is 7.1 ppm/°C, very close to the CTE of Mg_2Si. The small variation in the thermal expansion behavior

at about 160−170 °C corresponds to the phase transition of ZrW_2O_8. The difference in CTE between high temperatures and low temperatures is less than 1 ppm/°C, so it is not likely to negatively affect the thermal stability of the junction between the composite and the thermoelectric or the semiconductor material.

An interesting effect of the ZrW_2O_8 content is that it is possible for the composite to exhibit an inversion in the CTE value from negative to positive when the zirconium tungstate undergoes the phase change. This behavior will occur for composites containing large zirconium tungstate amounts, more than 50 vol %.

As an example, a sample containing 64% of ZrW_2O_8 has an average CTE of 0.5 ± 1.3 ppm/°C measured between 80 and 300 °C; however, the average CTE in the 80−150 °C temperature range is slightly negative (−0.5 ppm/°C), while the average in the 180−300 °C temperature range is positive (around 2 ppm/°C). This inversion has been observed previously, and it is consistent with the phase transformation of zirconium tungstate and the related variation in the CTE of the ceramic.[61] It is important to underscore the point that at such large zirconium tungstate loadings it becomes harder to identify a reliable value for the CTE since a linear variation in length with temperature is not readily observed.

3.3. Electrical Properties. Electrical conductivity of the composites was measured using the van der Pauw method. The results are reported in Figure 7 and in Table S5 in the

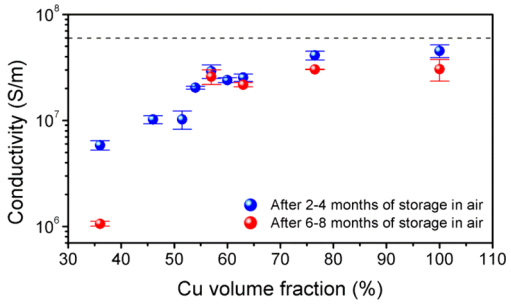

Figure 7. Average electrical conductivity as a function of the Cu volume fraction for the prepared samples. The expected value for bulk, fully dense copper (5.96×10^7 S/m) is highlighted with a dashed line.

Supporting Information. Each sample has been tested several times at room temperature (24 °C), and the different measurements were averaged into one value, using one standard deviation as the error.

The conductivity of pure Cu pellets averages about 75% of the conductivity of bulk copper, with the best samples reaching 85−90% of the bulk value of $\sim 6 \times 10^7$ S/m. These results are an indication of the high quality of the prepared materials and the ability to achieve bulk-like material properties at pressing temperatures as low as 500 °C. As expected, the conductivity decreases steadily with the amount of oxide filler; however, the composite samples are still very conductive. For example, the conductivity of samples containing up to 43 vol % of ZrW_2O_8 is more than 40% of the value of bulk Cu, while samples containing 60 vol % or more of oxide show conductivity values around 5.8×10^6 S/m, comparable to pure metals such as titanium ($\sim 2.5 \times 10^6$ S/m) and steels (between 1.5×10^6 S/m and 7×10^6 S/m).[62] Samples tested after several months of storage in air at room temperature (red dots in Figure 7) exhibit a drop in conductivity. Those metal−matrix composites with >50 vol % of Cu exhibit a small change, while the sample tested with <40 vol % Cu exhibited nearly a 10-fold decrease in conductivity from storage. Progressive oxidation in air at room temperature might be the reason for the observed drop in conductivity: the effect is more pronounced for samples where the amount of copper is closer to the percolation threshold for conduction.

The high conductivity values, along with the tunability of the CTE, make the metal−matrix composites suitable for a variety of applications in which the device has to be thermally cycled, where good electrical contact must be maintained and problems with thermomechanical stresses must be avoided.

3.4. Thermal Properties. In view of the high values for the electrical conductivity, it is not surprising that the metal−matrix composites exhibit high thermal conductivities. Figure 8 shows

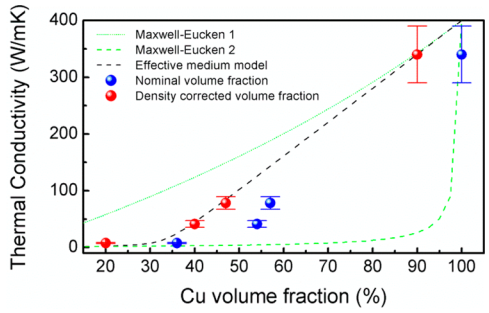

Figure 8. Thermal conductivity as a function of the Cu volume fraction for the prepared samples. The values predicted with the effective medium model (dashed black line) and with the Maxwell−Eucken model (dotted and dashed green lines for the upper and lower limit, respectively) are also shown. The thermal conductivity of pure Cu is ~400 W/mK.

the measured and predicted thermal conductivities of the composite pellets at room temperature as a function of the volume fraction of copper. Without the oxide filler, the measured thermal conductivity of the composite is 340 W/mK, which is about 85% of the expected value for bulk copper (401 W/mK). The thermal conductivity decreases steadily with increasing zirconium tungstate loading in the composite formulation, as expected. We compared the experimental data with predictions from two different models: the Maxwell−Eucken model and the effective medium model.

The Maxwell−Eucken model assumes that the dispersed component does not form continuous conduction pathways, and it therefore gives an upper and a lower bound to the composite thermal conductivities. The model considers either (i) that the fillers are isolated from each other and the Cu matrix provides continuous, highly heat conductive paths (upper limit), or (ii) that the fillers themselves form continuous, highly insulating paths and that the conductive Cu regions are isolated from each other (lower limit).

The effective medium model (EMM) represents a heterogeneous material where the two components are distributed randomly and either of them may form continuous conduction pathways. More detailed explanations of the two models can be found elsewhere.[63]

As shown in Figure 8, the experimental data (blue dots) seem to follow the trend of EMM predictions, but there is a horizontal shift compared to the model prediction due to finite amounts of porosity as indicated in the density measurements (see Figure 4). When the volume fraction of copper is

corrected after taking into account the porosity of the samples as evaluated from the density measurements, we obtain good agreement between the measured thermal conductivity and the predictions of the EMM (red dots in Figure 8).

CONCLUSIONS

We have developed metal−matrix composites which possess high electrical and thermal conductivities in combination with tunable thermal expansion coefficients. The continuous copper matrix is responsible for the electrical and thermal conductivity properties, while the addition of ZrW_2O_8, a negative thermal expansion material, enables us to vary the CTE in a predictable and reproducible fashion by more than a factor of 10, from <1 ppm/°C to the value of pure copper. A key feature which is essential in fabricating these materials is the use of hot-pressing conditions which avoid the decomposition of the ZrW_2O_8. To achieve the mild conditions of 500 °C for 1 h at 40 MPa, we take advantage of the lower sintering temperatures, especially of metals, which occur upon decreasing particle size to the nanodimensional range. Accordingly, we developed a synthetic route for the preparation of Cu NPs based on the reduction of a common copper salt in aqueous solution using PVP as a stabilizer and size-controlling agent. The improved thermomechanical reliability which results from this unique combination of high electrical and thermal conductivities and low thermal expansion enables these Cu-based metal−matrix composites to be used as electrical contacts to a variety of semiconductor and thermoelectric devices which can be operated under thermal cycling conditions.

ASSOCIATED CONTENT

Supporting Information

Additional characterizations and data: Figure S1−S5 and Table S1−S5. This material is available free of charge via the Internet at http://pubs.acs.org.

AUTHOR INFORMATION

Corresponding Author

*E-mail: bdunn@ucla.edu.

Present Address

[‖]Materials Science and Engineering, CSIRO, Bayview Avenue, Clayton, Victoria, 3168, Australia.

Author Contributions

Each author gave a significant contribution to the experiments described and to the manuscript preparation. All authors have given approval to the final version of the manuscript.

Notes

The authors declare no competing financial interest.

ACKNOWLEDGMENTS

This material is based upon work supported by the National Science Foundation and the Department of Energy under Grant No. CBET-1048726. The authors would like to thank Hyungseok Kim and Jesse Ko for TEM images and XRD measurements.

REFERENCES

(1) Hatzikraniotis, E.; Zorbas, K. T.; Samaras, I.; Kyratsi, T.; Paraskevopoulos, K. M. *J. Electron. Mater.* **2010**, *39*, 2112−2116.
(2) Barako, M. T.; Park, W.; Marconnet, A. M.; Asheghi, M.; Goodson, K. E. *J. Electron. Mater.* **2013**, *42*, 372−381.
(3) Ravi, V.; Firdosy, S.; Caillat, T.; Brandon, E.; Walde, K. V. D.; Maricic, L.; Sayir, A. *J. Electron. Mater.* **2009**, *38*, 1433−1442.
(4) Kondoh, K.; Oginuma, H.; Tuzuki, R.; Aizawa, T. *Mater. Trans.* **2003**, *44*, 611−618.
(5) Thakur, S. K.; Dhindaw, B. K.; Hort, N.; Kainer, K. U. *Metall. Mater. Trans. A* **2004**, *35*, 1167−1176.
(6) Herz, K.; Powalla, M.; Eicke, A. *Phys. Status Solidi A* **1994**, *145*, 415−424.
(7) Muller, E.; Drasar, C.; Schliz, J.; Kaysser, W. A. *Mater. Sci. Eng. A* **2003**, *362*, 17−39.
(8) Adachi, S. In *GaAs and Related Materials: Bulk Semiconducting and Superlattice Properties*; World Scientific: River Edge, NJ, 1994; p 38.
(9) Glazov, V. M.; Pashinkin, A. S. *Inorg. Mater.* **2000**, *36*, 225−231.
(10) Haruna, K.; Maeta, H.; Ohashi, K.; Koike, T. *J. Phys. C: Solid State Phys.* **1987**, *20*, 5275−5279.
(11) Deus, P.; Schneider, H. A.; Voland, U.; Stiehler, K. *Phys. Status Solidi A* **1987**, *103*, 443−447.
(12) Lide, D. R. In *CRC Handbook of Chemistry and Physics*, 87th ed.; Taylor and Francis: Boca Raton, FL, 2007; pp 12−196, 12−197.
(13) Ibrahim, I. A.; Mohamed, F. A.; Lavernia, E. J. *J. Mater. Sci.* **1991**, *26*, 1137−1156.
(14) Lloyd, D. J. *Int. Mater. Rev.* **1994**, *39*, 1−23.
(15) Miracle, D. B. *Compos. Sci. Technol.* **2005**, *65*, 2526−2540.
(16) Vaidya, R. U.; Chawla, K. K. *Compos. Sci. Technol.* **1994**, *50*, 13−22.
(17) Shen, Y. L.; Needleman, A.; Suresh, S. *Metall. Mater. Trans. A* **1994**, *25A*, 839−850.
(18) Elomari, S.; Skibo, M. D.; Sundarrajan, A.; Richards, H. *Compos. Sci. Technol.* **1998**, *58*, 369−376.
(19) Mary, T. A.; Evans, J. S. O.; Vogt, T.; Sleight, A. W. *Science* **1996**, *272*, 90−92.
(20) Evans, J. S. O.; Mary, T. A.; Vogt, T.; Subramanian, M. A.; Sleight, A. W. *Chem. Mater.* **1996**, *8*, 2809−2823.
(21) Tucker, M. G.; Goodwin, A. L.; Dove, M. T.; Keen, D. A.; Wells, S. A.; Evans, J. S. O. *Phys. Rev. Lett.* **2005**, *95*, 255501.
(22) Barrera, G. D.; Bruno, J. A. O.; Barron, T. H. K.; Allan, N. L. *J. Phys.: Condens. Matter* **2005**, *17*, R217−R252.
(23) Mancheva, M. N.; Iordanova, R. S.; Dimitriev, Y. B.; Petrov, K. P.; Avdeev, G. V. *J. Phys. Chem. C* **2007**, *111*, 14945−14947.
(24) Perottoni, C. A.; da Jornada, J. A. H. *Science* **1998**, *280*, 886−889.
(25) Gallardo-Amores, J. M.; Amador, U.; Moran, E.; Alario-Franco, M. A. *Int. J. Inorg. Mater.* **2000**, *2*, 123−129.
(26) Arora, A. K.; Sastry, V. S.; Sahu, P. C.; Mary, T. A. *J. Phys.: Condens. Matter* **2004**, *16*, 1025−1031.
(27) Evans, J. S. O.; Hu, Z.; Jorgensen, J. D.; Argyriou, D. N.; Short, S.; Sleight, A. W. *Science* **1997**, *275*, 61−65.
(28) Liang, E. J. *Recent Pat. Mater. Sci.* **2010**, *3*, 106−128.
(29) Verdon, C.; Dunand, D. C. *Scr. Mater.* **1997**, *36*, 1075−1080.
(30) Holzer, H.; Dunand, D. C. *J. Mater. Res.* **1999**, *14*, 780−789.
(31) Jakubinek, M. B.; Whitman, C. A.; White, M. A. *J. Therm. Anal. Calorim.* **2010**, *99*, 165−172.
(32) Trujillo, J. E.; Kim, J. W.; Lan, E. H.; Sharratt, S.; Ju, Y. S.; Dunn, B. *J. Electron. Mater.* **2012**, *41*, 1020−1023.
(33) Lai, S. L.; Guo, J. Y.; Petrova, V.; Ramanath, G.; Allen, L. H. *Phys. Rev. Lett.* **1996**, *77*, 99−102.
(34) Nanda, K. K.; Maisels, A.; Kruis, F. E.; Fissan, H.; Stappert, S. *Phys. Rev. Lett.* **2003**, *91*, 106102.
(35) Arcidiacono, S.; Bieri, N. R.; Poulikakos, D.; Grigoropoulos, C. P. *Int. J. Multiphase Flow* **2004**, *30*, 979−994.
(36) Safaei, A.; Shandiz, M. A.; Sanjabi, S.; Barber, Z. *J. Phys. Chem. C* **2008**, *112*, 99−105.
(37) Lide, D. R. In *CRC Handbook of Chemistry and Physics*, 87th ed.; Taylor and Francis: Boca Raton, FL, 2007; pp 12−39, 12−40.
(38) DeBuysser, K.; Smet, P. F.; Schoofs, B.; Bruneel, E.; Poelman, D.; Hoste, S.; Van Driessche, I. *J. Sol-Gel Sci. Technol.* **2007**, *43*, 347−353.
(39) Hao, E.; Lian, T. *Chem. Mater.* **2000**, *12*, 3392−3396.

(40) Glavee, G. N.; Klabunde, K. J.; Sorensen, C. M.; Hadjapanayis, G. C. *Langmuir* **1992**, *8*, 771−773.
(41) Prikhodko, S. V.; Ardell, A. J. *Acta Mater.* **2003**, *51*, 5001−5012.
(42) ImageJ. http://rsb.info.nih.gov/ij (accessed 25/09/2013).
(43) McCormack, J. A.; Fleurial, J. P. In *Modern Perspectives on Thermoelectrics and Related Materials, MRS Symp. Proc.*, Materials Research Society: Warrendale, PA, 1991; Vol. *234*, p 135.
(44) Behera, M.; Ram, S. *Int. Nano Lett.* **2013**, *3*, 17.
(45) Tsunoyama, H.; Sakurai, H.; Ichikuni, N.; Negishi, Y.; Tsukuda, T. *Langmuir* **2004**, *20*, 11293−11296.
(46) Guo, L.; Huang, Q. J.; Li, X. Y.; Yang, S. *Langmuir* **2006**, *22*, 7867−7872.
(47) Couto, G. G.; Klein, J. J.; Schreiner, W. H.; Mosca, D. H.; de Oliveira, A. J. A.; Zarbin, A. J. G. *J. Colloid Interface Sci.* **2007**, *311*, 461−468.
(48) Yu, W.; Xie, H.; Chen, L.; Li, Y.; Zhang, C. *Nanoscale Res. Lett.* **2009**, *4*, 465−470.
(49) Sun, Y.; Mayers, B.; Xia, Y. *Nano Lett.* **2003**, *3*, 675−679.
(50) Métraux, G. S.; Mirkin, C. A. *Adv. Mater.* **2005**, *17*, 412−415.
(51) Yin, M.; Wu, C. K.; Lou, Y.; Burda, C.; Koberstein, J. T.; Zhu, Y.; O'Brien, S. *J. Am. Chem. Soc.* **2005**, *127*, 9506−9511.
(52) Rice, K. P.; Walker, E. J., Jr.; Stoykovich, M. P.; Saunders, A. E. *J. Phys. Chem. C* **2011**, *115*, 1793−1799.
(53) Alvarez, M. M.; Khoury, J. T.; Schaaff, T. G.; Shafigullin, M. N.; Vezmar, I.; Whetten, R. L. *J. Phys. Chem. B* **1997**, *101*, 3706−3712.
(54) Liz-Marzan, L. M.; Giersig, M.; Mulvaney, P. *Langmuir* **1996**, *12*, 4329−4335.
(55) Kozy, L. C.; Nawaz Tahir, M.; Lind, C.; Tremel, W. *J. Mater. Chem.* **2009**, *19*, 2760−2765.
(56) Banek, N. A.; Baiz, H. I.; Latigo, A.; Lind, C. *J. Am. Chem. Soc.* **2010**, *132*, 8278−8279.
(57) Wu, H.; Badrinarayanan, P.; Kessler, M. R. *J. Am. Ceram. Soc.* **2012**, *95*, 3643−3650.
(58) Yilmaz, S. *Compos. Sci. Technol.* **2002**, *62*, 1835−1839.
(59) Yilmaz, S.; Dunand, D. C. *Compos. Sci. Technol.* **2004**, *64*, 1895−1898.
(60) Wu, Y.; Wang, M.; Chen, Z.; Ma, N.; Wang, H. *J. Mater. Sci.* **2013**, *48*, 2928−2933.
(61) Balch, D. K.; Dunand, D. C. *Metall. Mater. Trans. A* **2004**, *35A*, 1159−1165.
(62) Lide, D. R. In *CRC Handbook of Chemistry and Physics*, 87th ed.; Taylor and Francis: Boca Raton, FL, 2007; pp 12−211.
(63) Carson, J. K.; Lovatt, S. J.; Tanner, D. J.; Cleland, A. C. *Int. J. Heat Mass Transfer* **2005**, *48*, 2150−2158.